Fabrication of topographically microstructured titanium silicide interface for advanced photonic applications

M. Hannula[a], K. Lahtonen[a], H. Ali-Löytty[a], A.A. Zakharov[b], T. Isotalo[a], J. Saari[a], M. Valden[a,*]

[a]*Surface Science Laboratory, Optoelectronics Research Centre, Tampere University of Technology, P.O. Box 692, FI-33101 Tampere, Finland*
[b]*MAX IV Laboratory, Lund University, P.O. Box 118, SE-22100 Lund, Sweden*

Abstract

We present a widely scalable, high temperature post-growth annealing method for converting ultra-thin films of TiO_2 grown by atomic layer deposition to topographically microstructured titanium silicide (TiSi). The photoemission electron microscopy results reveal that the transformation from TiO_2 to TiSi at 950 °C proceeds via island formation. Inside the islands, TiO_2 reduction and Si diffusion play important roles in the formation of the highly topographically microstructured TiSi interface with laterally nonuniform barrier height contact. This is advantageous for efficient charge transfer in Si-based heterostructures for photovoltaic and photoelectrochemical applications.

Keywords: Atomic layer deposition (ALD), X-ray photoelectron spectroscopy (XPS), Transition metal silicides, Semiconductors, Surface modification

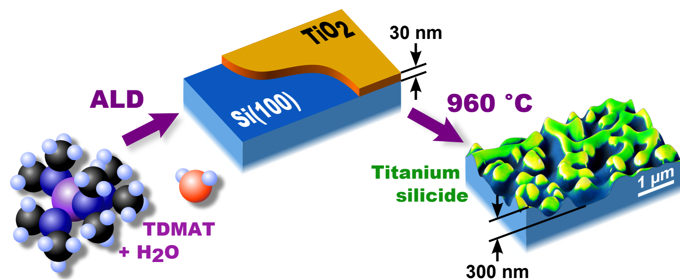

*Corresponding author
Email address: mika.valden@tut.fi (M. Valden)
URL: www.tut.fi/surfsci (M. Valden)

Titanium silicide (TiSi) nanostructures have been widely used in nano- and microelectronics as ohmic contacts and interconnect materials [1] and, in recent years, photoelectrochemical (PEC) devices developed for water splitting [2, 3, 4]. TiSi has an exceptionally broad band-gap from 1.5 eV to 3.4 eV that is alone large enough to allow photocatalytical splitting of water [4]. The efficiency of a PEC device can be increased by interfacing a semiconductor material with an electrocatalyst (EC). Key parameters in the optimization of PEC materials for water splitting are the electronic band positions with respect to water redox potentials. Under electrolyte contact, the Fermi levels of a photoelectrode and electrolyte redox species align via charge transfer resulting in band bending within the semiconductor photoelectrode. If an EC covers a semiconductor substrate completely, the electronic band alignment is determined by the EC. In contrast, if the EC layer is discontinuous, the band alignment can behave like the semiconductor but the surface has the catalytic activity of the EC. Based on the "pinch-off" theory this behavior is valid for catalyst particles with dimensions smaller than the depletion width of the semiconductor [5]. The depletion width is strongly affected by the degree of free charge carriers, and is in the range of few micrometers for a lightly doped Si [6].

Here we demonstrate a simple atomic layer deposition (ALD) and thermal annealing based method for fabricating a topographically microstructured discontinuous TiSi surface on Si substrate. This allows for energy band engineering of photoelectrodes via exploitation of the pinch-off effect. Hill et al. recently showed that the pinch-off effect produced by cobalt silicide heterostructures grown on silicon photoanodes can significantly improve their PEC performance [7]. The ALD process described in the present study is envisaged being a generic technological approach to the fabrication of metal silicide particles (e.g. TiSi, CoSi, NiSi) on Si [1, 8, 9].

In this study TiSi is fabricated from ALD grown TiO_2 ultra-thin film which is extremely conformal and homogenous. The film is transformed into TiSi by post-annealing which also makes it thermally stable for subsequent film depositions. Our results reveal the initial stages of the island mediated process where the titanium dioxide ultra-thin film undergoes a transformation to suboxides and subsequently to titanium silicide. Furthermore, the laterally resolved chemical composition of the resulting microstructured TiSi surface texture is analyzed.

The phosphorus doped (resistivity 1–20 Ω·cm) n-type Si(100) wafers were purchased from Wafer World, Inc. (Florida, USA). The 400 μm thick, three inch diameter pre-polished wafers had been cut in (100) orientation with ± 1 ° accuracy. For the experiments 10×10 mm^2 squares were cleaved. The details of the annealing and hydrogen plasma based in

situ cleaning of the silicon substrates are described in the Supplementary Material. The cleaned silicon substrates were transferred ex situ to Picosun Sunale ALD R200 Advanced reactor for titanium oxide deposition. The air exposure during the sample transfer was kept as short as possible, approximately 5 min.

40 ALD of titanium dioxide was carried out at a substrate temperature of 200 °C. Deposition consisted of 804 cycles of tetrakis(dimethylamido)titanium(IV) (TDMAT) and deionized water leading to a film thickness of 28.7±0.3 nm as verified by ellipsometry (see Supplementary Material). After the deposition the samples were cooled down in N_2 atmosphere before transferring them back to UHV for high temperature annealing.

45 Two separate UHV systems with a base pressure below $1{\times}10^{-10}$ mbar were employed for annealing and subsequent electron spectroscopy experiments. X-ray photoelectron spectroscopy (XPS) and energy filtered photoemission electron microscopy (EF-PEEM) measurements were carried out using NanoESCA (Omicron NanoTechnology GmbH) spectromicroscopy system [10]. Focused monochromatized Al Kα radiation ($h\nu$ = 1486.5 eV)
50 was utilized for core level spectroscopy and imaging whereas secondary electron tail cut-off maps for work function determination were measured with non-monochromatized He Iα radiation ($h\nu$ = 21.22 eV) using HIS 13 VUV Source (Focus GmbH). The XP spectra were collected using a hemispherical analyzer with energy resolution of 400 meV or 50 meV (for high resolution (HR) XPS). For EF-PEEM measurements the energy resolution of an
55 aberration correcting double hemispherical energy analyzer (IDEA) was set to 800 meV for core level imaging and 50 meV for secondary electron imaging. Lateral resolution for core level images was approximately 500 nm and for He Iα excited secondary electron images approximately 100 nm.

High spatial resolution EF-PEEM measurements were performed with a spectroscopic
60 photoemission and low energy electron microscope (SPELEEM) III (Elmitech GmbH) [11] at the soft X-ray beamline I311 of MAX II storage ring in the MAX IV Laboratory synchrotron radiation (SR) facility (Lund, Sweden) [12]. SPELEEM was utilized in photoelectron emission, low energy electron microscopy (LEEM) and imaging X-ray absorption (XAS) secondary electron yield modes.

65 In addition to XPS and EF-PEEM studies the surface morphology of the 950 °C annealed island structured sample was studied by scanning electron microscopy (SEM; Zeiss Ultra 55, Carl Zeiss Microscopy GmbH) and atomic force microscopy (AFM; Veeco Dimension 3100 AFM, Veeco Instruments Inc.).

Both NanoESCA and SPELEEM III had a heating assembly in their preparation cham-
70 bers for heat treatments of the samples. For studies performed in the NanoESCA system

the ALD grown TiO_2 was initially annealed at 950 °C for 10 min to form titanium silicide islands. Studying the edge areas of these islands with PEEM revealed details of the reduction process involved in the transformation of titanium (sub)oxides to titanium silicide. Subsequently the sample was annealed to 960 °C for 10 min to reduce the remaining
75 titanium oxide areas to continuous titanium silicide ridge-like microstructure.

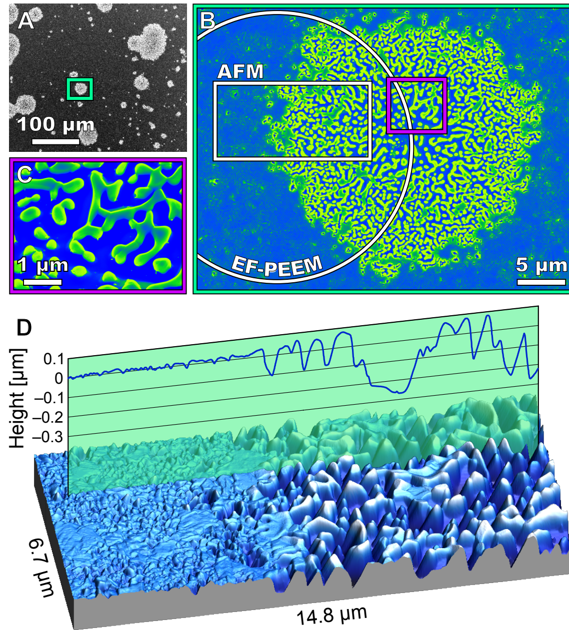

Figure 1: A–C: SEM images of a highly topographically microstructured TiSi island after 950 °C annealing. Highest magnification in Fig. C shows the detailed TiSi ridge-like microstructure inside the island. The white circle in Fig. B shows the area selected for EF-PEEM studies and will be discussed later in detail. D: AFM image of the region framed with a white rectangle in Fig. B. AFM line profile illustrates the abrupt change in TiO_x surface topography when moving from the area outside the island (left side) to the heavily corrugated ridge-like area inside the island (right side).

SEM images in Figs. 1A–C illustrate the TiSi island structure after the 950 °C annealing. Islands nucleate at seemingly random locations and with inhomogeneous size distribution. The ALD grown TiO_2 film is homogenous, and therefore it is likely that the nucleation has been initiated by small impurity particles or crystal defects in the Si sub-
80 strate. It is noteworthy that the nucleation does not happen instantaneously but requires 5 to 10 minutes at 950 °C temperature. Temperatures of 920 °C and below were also tested but this only resulted in titanium suboxide formation without any indication of silicidation or evolution of island structures.

SEM images show distinct ridge-like microstructures inside the islands. Thus the true
85 topography around a selected island was studied by AFM. Fig. 1D demonstrates that the

remaining titanium (sub)oxide film outside the island has retained a smooth surface with a roughness value Ra of 8.0 ± 0.5 nm. However, inside the islands the roughness has increased to 79 ± 2 nm with maximum height variations of more than 300 nm which is ten times the thickness of the original TiO_2 film. Also the average height of the surface was approximately 40 nm lower in comparison with the surrounding partly reduced, but not silicidized, TiO_x surface. This suggests that the annealing process not only affects the TiO_2 film but also induces pronounced mass transfer in the silicon substrate by means of diffusion, corrugation and desorption. According to Zhao et al. [13] silicon from the substrate diffuses to titanium overlayer where it reacts with oxygen and sublimates as silicon monoxide. In our case, the titanium film has abundance of available oxygen released by the TiO_x reduction process.

An interesting detail in Figs. 1B and C is that the TiSi ridges near the center of the island, i.e. near the initial nucleation point, are small and almost spherical. When diverging from the center, the ridges became more elongated and interconnected. For both shapes the width of the structures is similar, approximately 200–300 nm. The constant width of the ridges could be explained with the shape stability of the clusters [14]. For small cluster the symmetrical compact shape is energetically favorable but as the cluster volume increases the growth proceeds preferably along the longitudinal direction thus increasing the aspect ratio.

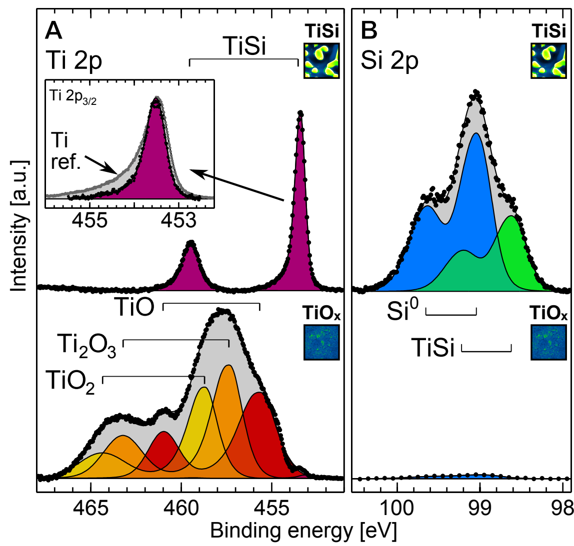

Figure 2: Ti 2p and Si 2p XPS core level spectra of a titanium silicide island (top) and the TiO_x surface surrounding the island (bottom). The gray peak behind the Ti $2p_{3/2}$ TiSi spectrum in the inset is measured from a clean Ti reference sample thus showing that the FWHM of Ti $2p_{3/2}$ peak has decreased in titanium silicide.

The chemical composition of the islands was studied by XPS. Figs. 2A and B show

105 the Ti 2p and Si 2p spectra measured inside the TiSi island and on the titanium suboxide surface between the islands. The surface between the islands is a combination of the original titanium dioxide and annealing induced suboxides. Three different oxidized states were identified corresponding to TiO_2 (458.7 eV), Ti_2O_3 (457.3 eV) and TiO (455.6 eV). Inside the islands titanium is completely reduced showing only the TiSi related component

110 at 453.4 eV. The full width at half maximum (FWHM) of the Ti $2p_{3/2}$ spectrum inside the silicidized regions has decreased from 0.57 eV of clean Ti to 0.48 eV in TiSi which is in accordance with the observations by Tam et al. [15]. However, in contrast to their study, no chemical shift in Ti 2p between clean Ti and TiSi was observed. On the other hand, Si 2p shows a 0.42 eV shift to lower binding energy. This behavior agrees with the results

115 from Palacio and Arranz [16] and thus consolidates the silicidation process on the islands. Also, all oxygen had desorbed from the islands.

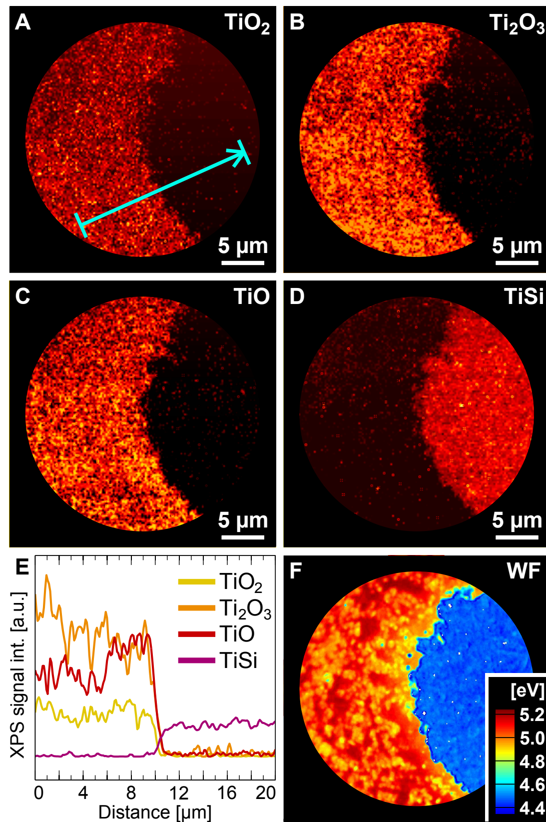

Figure 3: A–D: Chemical state resolved EF-PEEM images of the Ti 2p. Region of interest selected from the left side of the island in Fig. 1B. E: XPS signal intensity line profiles for each titanium compound. The profile position is indicated by the blue arrow in A and the line segments at the ends of the arrow represent the line width used for averaging the signal. F: Surface electronic state resolved image (Work Function contrast).

To obtain more localized information about the chemical composition of the island structure, EF-PEEM measurements of were conducted. The region of interest was selected from the left side of the island shown in Fig. 1B and images as a function of kinetic
120 energy were recorded with a 29 μm field of view. For the analysis the image series was first energy dispersion corrected using a clean Si(100) substrate as a flat field reference (see Supplementary Material). After this the data was noise filtered using principal component analysis (PCA) with four abstract factors. Finally, the image stack was deconvoluted pixel-by-pixel to different chemical states using the components in Fig. 2A as a reference.

125 The chemical state resolved images of the Ti 2p transition (Fig. 3A–D) show an extremely sharp transformation interface between the titanium suboxide and silicide regions. Line profiles were extracted from the position indicated by the blue arrow in Fig. 3A. TiO_2 and Ti_2O_3 show relatively homogenous distribution when approaching the island edge. However, the TiO signal increases 4 μm before the edge. This can be interpreted
130 to indicate that the island growth proceeds via a TiO rich rim which expands together with the island edge. In addition, no silicon diffusion through the oxide film was observed. This is in contrast with experiments performed on metallic Ti/Si surfaces where diffusion is reported already at 400–800 °C [17, 18, 19].

The work function (WF) of the silicide island and the surrounding Ti suboxide region
135 was determined by measuring the distance of secondary electron cut-off edge from the Fermi level. Figure 3F shows a 0.6–0.8 eV decrease in WF inside the silicidized region. The WF inside the silicidized region is to a large extent homogeneous and corresponds to the WF of a clean Si(100) reference. In particular, the slight variation of the WF does not coincide with the TiSi particle distribution, which supports the pinch-off effect. The
140 lowered WF value can be utilized in ohmic contacts to adjust the Schottky barrier height which is particularly important due to the efficient charge-transport properties of TiSi in nanoelectronics and solar energy harvesting applications [4].

Lateral resolution in core level imaging performed by the NanoESCA system is limited to approximately 500 nm. However, the SEM and AFM images revealed internal submi-
145 crometer scale structures inside the silicide islands. To better understand the chemistry of these structural features another TiO_2/Si sample was annealed to 960 °C and studied by SR-EF-PEEM which can achieve a lateral resolution down to 40 nm [20]. The increase in annealing temperature from 950 °C to 960 °C completed the reduction process causing the TiSi islands to coalesce into the highly topographically microstructured TiSi ridge pattern
150 covering the whole Si substrate (Fig. 4). An SR-EF-PEEM image series of Si 2p region was recorded and deconvoluted to elemental silicon and TiSi states based on the components in

Fig. 2B. For titanium a corresponding image series was recorded using XAS in secondary electron yield mode and the titanium distribution was determined from the area of the Ti L_{III} peak area in each pixel. The insets in Fig. 4 show a clear correspondence between Si_{TiSi} and Ti. In addition, these signals originate from the areas which are observed as high ridges in SEM and AFM images. However, there is some Ti left also in the depressions (Fig S1). This has not been identified in previous studies on metallic Ti–Si/SiO_2 systems which claim that the valleys are composed of pure silicon [21, 22]. Aside from the slight difference in the initial conditions, this discrepancy could be explained by the use of XAS in secondary electron mode with decreased surface sensitivity. Thus it can not be concluded whether the remaining titanium in the depressions is on the surface or buried deeper inside the silicon.

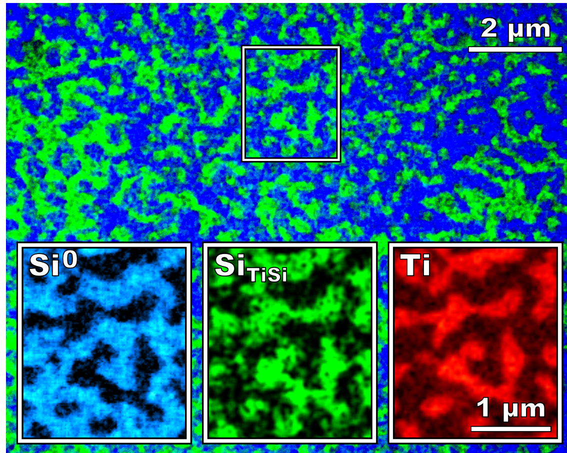

Figure 4: SR-EF-PEEM image of the topographically microstructured TiSi ridge pattern after annealing to 960 °C. Blue and green areas correspond to elemental silicon and silicon in TiSi, respectively (see Fig. 2B for peak reference). Insets show a magnified view of both silicon chemical states together with the Ti XAS signal from the same area.

Low energy electron diffraction (LEED) measurement of the silicidized surface showed a 2×1 pattern typical for reconstructed Si(100). The pattern was, however, much dimmer and with a high background intensity (Fig. S2) when compared to the LEED pattern that was measured from the UHV cleaned Si(100). The 2×1 intensity maxima showed replicas which could be attributed to the lattice distortion produced by the Ti atoms in the valleys. However, the pattern did not show any new maxima which suggests that the surface structure of the TiSi ridges has no clear long range order. The same conclusion was obtained from the LEEM images (not shown) that showed the (0,0) diffraction maximum for the valley regions but not for the TiSi ridges.

The formation of the highly topographically microstructured TiSi surface phase can be

explained based on the total surface and bulk energy minimization. The classical nucleation theory suggests that in most cases the surface energy increases and the bulk energy decreases with increasing cluster size. The total free energy is the sum of these two and can be reduced by the formation of larger clusters. [21] Cluster formation requires that sufficient energy is available for overcoming the nucleation barrier. According to Hyeongtag et al. [19] the nucleation barrier is higher for C54 $TiSi_2$ phase than C49 $TiSi_2$. Based on their results the ≥ 950 °C annealing is, however, sufficient for the formation of the thermodynamically more stable C54 $TiSi_2$ phase. This phase is also more desirable for photoelectrochemical applications, such as photoanodes used in water oxidation, due to its lower resistivity.

In order to study the chemical stability of the silicidized surface it was exposed to air (1 ATM) for 48 h. Only 28 % of the silicidized titanium oxidized back to Ti^{4+} (25 %) and Ti^{3+} (3 %). On a clean Ti reference surface 77 % of titanium became oxidized during the same oxidation treatment. This high oxidation resistance in ambient conditions can be seen as one of the key factors that make TiSi compounds so widely exploited in semiconductor industry.

In summary, we have demonstrated a widely scalable method for synthesizing a highly topographically microstructured titanium silicide texture on silicon substrates which allows for energy band engineering of Si based photoelectrodes via the exploitation of the pinch-off effect. The synthesis is based on vacuum post-annealing of ALD grown TiO_2 ultra-thin film and can thus be implemented inside one processing chamber. This makes the TiSi fabrication feasible in production chains that include several consecutive conformal coatings used in e.g. surface protection, passivation or formation of catalytically active surface/interface layer. The presented synthesis route opens up the possibility for new state-of-the-art interface engineering for photoelectrochemical devices and nano- and microelectronics.

The authors acknowledge the TUT's Graduate School. We also acknowledge financial support by the Academy of Finland (decision numbers 141481 and 286713) and by KAUTE foundation. We are grateful to the staff of the MAX IV laboratory for affording the use of the research facilities.

References

[1] S.-L. Zhang, M. Östling, Critical Reviews in Solid State and Materials Sciences 28 (2003) 1–129. doi:10.1080/10408430390802431.

205 [2] S. Banerjee, S. K. Mohapatra, M. Misra, The Journal of Physical Chemistry C 115 (2011) 12643–12649. doi:10.1021/jp106879p.

[3] Y. Lin, S. Zhou, X. Liu, S. Sheehan, D. Wang, Journal of the American Chemical Society 131 (2009) 2772–2773. doi:10.1021/ja808426h.

[4] P. Ritterskamp, A. Kuklya, M.-A. Wüstkamp, K. Kerpen, C. Weidenthaler, M. Demuth, Angewandte Chemie International Edition 46 (2007) 7770–7774. doi:10.1002/anie.200701626.

[5] R. C. Rossi, N. S. Lewis, The Journal of Physical Chemistry B 105 (2001) 12303–12318. doi:10.1021/jp011861c.

[6] J.-P. Colinge, C. A. Colinge, Physics of Semiconductor Devices, Kluwer Academic Publishers, 2002. eBook ISBN: 9780306476228.

[7] J. C. Hill, A. T. Landers, J. A. Switzer, Nature Materials 14 (2015) 1150–1155. doi:10.1038/nmat4408.

[8] S. Hu, M. R. Shaner, J. A. Beardslee, M. Lichterman, B. S. Brunschwig, N. S. Lewis, Science 344 (2014) 1005–1009. doi:10.1126/science.1251428.

220 [9] M. J. Kenney, M. Gong, Y. Li, J. Z. Wu, J. Feng, M. Lanza, H. Dai, Science 342 (2013) 836–840. doi:10.1126/science.1241327.

[10] Omicron NanoTechnology NanoESCA, 2016. See www.scientaomicron.com for details of the instrument.

[11] Elmitec SPELEEM III, 2016. See www.elmitec.de for details of the instrument.

225 [12] R. Nyholm, J. Andersen, U. Johansson, B. Jensen, I. Lindau, Nuclear Instruments and Methods in Physics Research Section A: Accelerators, Spectrometers, Detectors and Associated Equipment 467468, Part 1 (2001) 520–524. doi:10.1016/S0168-9002(01)00399-0, 7th Int. Conf. on Synchrotron Radiation Instrumentation.

[13] F. Zhao, X. Cui, B. Wang, J. Hou, Applied Surface Science 253 (2006) 2785–2791. doi:10.1016/j.apsusc.2006.05.054.

[14] W.-C. Yang, H. Ade, R. J. Nemanich, Journal of Applied Physics 95 (2004) 1572–1576. doi:10.1063/1.1636526.

[15] P. Tam, Y. Cao, L. Nyborg, Surface Science 606 (2012) 329–336. doi:10.1016/j.susc.2011.10.015.

235 [16] C. Palacio, A. Arranz, Applied Surface Science 253 (2007) 4283–4288. doi:10.1016/j.apsusc.2006.09.031.

[17] S. Ogawa, T. Kouzaki, T. Yoshida, R. Sinclair, Journal of Applied Physics 70 (1991) 827–832. doi:10.1063/1.349641.

[18] C. Kim, S.-W. Kim, C.-H. Hong, D.-W. Kim, H.-K. Baik, C. Whang, Journal of
240 Crystal Growth 189–190 (1998) 720–724. doi:10.1016/S0022-0248(98)00270-X.

[19] H. Jeon, R. Nemanich, Thin Solid Films 184 (1990) 357–363. doi:10.1016/0040-6090(90)90432-D.

[20] The MAX IV Laboratory, 2016. See information about MAX II beamline I311: www.maxlab.lu.se.

245 [21] H. Jeon, C. A. Sukow, J. W. Honeycutt, G. A. Rozgonyi, R. J. Nemanich, Journal of Applied Physics 71 (1992) 4269–4276. doi:10.1063/1.350808.

[22] J. C. Barbour, A. E. M. J. Fischer, J. F. van der Veen, Journal of Applied Physics 62 (1987) 2582–2584. doi:10.1063/1.339433.